COMBINED MONTHLY PROGRESS REPORTS NOS. 1 - 4

Covering the Period

1 October 1969 - 31 January 1970

INVESTIGATION OF THE D AND E REGIONS OF THE IONOSPHERE

NASw-1994

L. G. Smith
Project Manager

GCA CORPORATION
GCA TECHNOLOGY DIVISION
Bedford, Massachusetts

Prepared for

NASA Headquarters
Washington, D. C.

I. INTRODUCTION

This investigation of the D and E-regions of the ionosphere is a continuation of a program conducted jointly with the University of Illinois. The GCA Technology Division effort has previously been conducted under contracts NASW-820, NASW-1141 and NASW-1402. A total of 38 launches of Nike Apache rockets has been accomplished between April 1964 and September 1969, as indicated in Table 1. Of these, 29 have been completely successful and four were complete failures (14.229, 14.272, 14.305 and 14.309). The remaining five are considered partially successful since useful scientific data were obtained from some of the experiments (14.248, 14.271, 14.302, 14.273 and 14.393).

The scientific objectives of these preceding programs have covered many areas. Some of the more important are: (1) Development of the ionosphere at sunrise, (2) seasonal variation at solar minimum, (3) latitudinal variation at solar minimum, (4) seasonal variation at solar maximum, (5) diurnal variation, (6) the structure of the nighttime ionosphere, (7) winter anomaly in the D-region, (8) Sporadic-E, (9) electron temperature of the E-region, and (10) O_2 and O_3 concentrations in the D-region.

The results of these investigation have been published by staff members of GCA Technology Division and of the University of Illinois, in some cases spearately, in others jointly.

The program is to be continued with an investigation of the ionosphere during the eclipse of 7 March 1970 and later in the year, an attempt to measure the electric field in a Sporadic-E layer. The effort of the period

TABLE 1

ROCKET LAUNCHES, GCA TECHNOLOGY DIVISION/UNIVERSITY OF ILLINOIS

Contract	Nike Apache	Time LST	Date	Place*	Remarks
NASW-820	14.143	1605	16 Apr. 1964	W.I.	$\chi = 60^{o}$
	14.144	0300	15 Jul. 1964	W.I.	predawn
	14.145	0420	15 Jul. 1964	W.I.	sunrise
	14.146	0525	15 Jul. 1964	W.I.	$\chi = 85^{o}$
	14.147	0607	10 Nov. 1964	W.I.	sunrise
	14.149	1520	19 Nov. 1964	W.I.	$\chi = 77^{o}$
	14.148	1702	19 Nov. 1964	W.I. (ship)	sunset
NASW-1141	14.228	0820	20 Mar. 1965	ship	$\chi = 60^{o}0^{o}$ mag
	14.229	0431	23 Mar. 1965	ship	TM failure
	14.230	0846	5 Apr. 1965	ship	$\chi = 60^{o}16^{o}$ mag
	14.231	1418	9 Apr. 1965	ship	$\chi = 60^{o}, 32^{o}$S mag
	14.232	1214	12 Apr. 1965	ship	$\chi = 67^{o}, 48^{o}$S mag
	14.245	0413	14 Jun. 1965	W.I.	$\chi = 95^{o}$
	14.246	1641	17 Jun. 1965	W.I.	$\chi = 60^{o}$
	14.244	1528	15 Sep. 1965	W.I.	$\chi = 60^{o}$
	14.247	1200	15 Dec. 1965	W.I.	$\chi = 60^{o}$
	14.248	1214	10 Jan. 1966	W.I.	partial TM failure
NASW-1402	14.270	0418	14 Jun. 1966	W.I.	$\chi = 95^{o}$
	14.271	1815	24 Aug. 1966	W.I.	$\chi = 85^{o}$
	14.272	1945	24 Aug. 1966	W.I.	TM failure
	14.274	1106	12 Nov. 1966	Brazil	eclipse
	14.302	1108	12 Nov. 1966	Brazil	eclipse
	14.304	1110	12 Nov. 1966	Brazil	eclipse
	14.303	1300	12 Nov. 1966	Brazil	post-eclipse
	14.275	1350	31 Jan. 1967	W.I.	$\chi = 60^{o}$
	14.273	1856	8 Aug. 1967	W.I.	MS failure
	14.308	1634	7 Sep. 1967	P.R.	$\chi = 60^{o}$
	14.305	2007	7 Sep. 1967	P.R.	TM failure
	14.309	0603	8 Sep. 1967	P.R.	vehicle failure
	14.358	0506	24 Jul. 1968	W.I.	$\chi = 90^{o}$
	14.359	0536	24 Jul. 1968	W.I.	$\chi = 85^{o}$
	14.360	1200	24 Jul. 1968	W.I.	noon
	14.361	1736	24 Jul. 1968	W.I.	$\chi = 60^{o}$
	14.391	1200	31 Jan. 1969	W.I.	$\chi = 55^{o}$
	14.392	1209	6 Feb. 1969	W.I.	$\chi = 53^{o}$
	14.393	1600	16 Apr. 1969	W.I.	partial instr. failure
	14.395	1546	10 Sep. 1969	W.I.	$\chi = 60^{o}$
	14.394	2306	11 Sep. 1969	W.I.	night

*W.I. = Wallops Island; ship = USNS Croatan; Brazil = Cassino, R.G. du Sol; P.R. = Puerto Rico.

reported here has been almost exclusively related to preparations for the eclipse rocket launches.

The total solar eclipse of 7 March 1970 presents an excellent opportunity for sounding rocket investigations. The launch site of the NASA Wallops Island facility is within the path of totality, and, as described in more detail in Section II, the circumstances of the eclipse are favorable for rocket launches into totality. The behavior of the ionosphere during a total (or nearly total) solar eclipse has long been recognized as a valuable source of information on the problem of ionization equilibrium. The earlier techniques, using ground-based radio propagation techniques were satisfactory for the E-regions and above but presented problems of interpretation in the lower part of the ionosphere. More recently, starting with the eclipse of 20 July 1963 and again in the eclipse of 12 November 1966, the ionosphere has been observed directly using rocket-borne probes. In this latter eclipse, the probe was combined with a propagation experiment to given excellent data on the D-region.

Though the variation of electron density has been the primary objective, other properties of the ionosphere and the ionizing radiations can, and have been investigated during solar eclipses. The variation of electron temperature in the E-region during an eclipse gives valuable insight into the problem of thermal equilibrium (or lack of it) between the temperature of electrons and the neutral atmosphere.

The observations of previous eclipses have supported the view that the ionosphere in the E-region remains in equilibrium during an eclipse, radiation from the solar corona in the X-ray region of the spectrum being the ionizing source. It is, therefore, important to observe the X-ray flux in some representative part of the spectrum. Other significant measurements of solar radiation flux that can be made with relatively simple instrumentation are those of Lyman-α (1216Å) and 2600Å. In addition, the absorption profiles of these two radiations give the concentrations of O_2 and O_3, respectively, in the D-region. The significance of these measurements is discussed in Section III.

The instrumentation for the payloads of the Nike Apache rockets is described in Section IV. The payloads require relatively little modification from those previously flown and are designed for economy, reliability and operational simplicity.

II. THE TOTAL SOLAR ECLIPSE OF 7 MARCH 1970

The path of totality of the solar eclipse of 7 March 1970 starts in the Pacific Ocean. It crosses Mexico and the Gulf of Mexico and reaches the U.S.A. in northern Florida, about 250 km east of the sounding rocket launch site at Eglin AFB. It travels northward along the coast of the southeastern states, leaving land in the vicinity of Norfolk, Virginia. The path crosses the eastern-most part of Massachusetts and Nova Scotia before ending in the North Atlantic Ocean. By a most remarkable chance, the launch facilities of the NASA Wallops Island Station are within the path of totality and, equally fortunately, the time of the eclipse there is close to mid-day.

The geographical situation in the vicinity of Wallops Island is shown in Figure 1. The locations of the main base (37.9333°N, 75.4667°W) and launch site (37.8380°N, 75.4829°W) are indicated. The main base is about 11 km north of the launch site. This separation is sufficient to put the main base 1 km outside, and the launch site 7 km inside the path of totality. The local circumstances for the eclipse at the main base are given in Table 2, in which χ is the solar zenith angle.

TABLE 2

LOCAL CIRCUMSTANCES AT WALLOPS ISLAND (MAIN BASE)

First Contact	1720:02.4 UT	$\chi = 43^\circ$
Maximum Phase	1837:59.3 UT	$\chi = 47^\circ$
Fourth Contact	1952:07.8 UT	$\chi = 57^\circ$

OICB334-20S

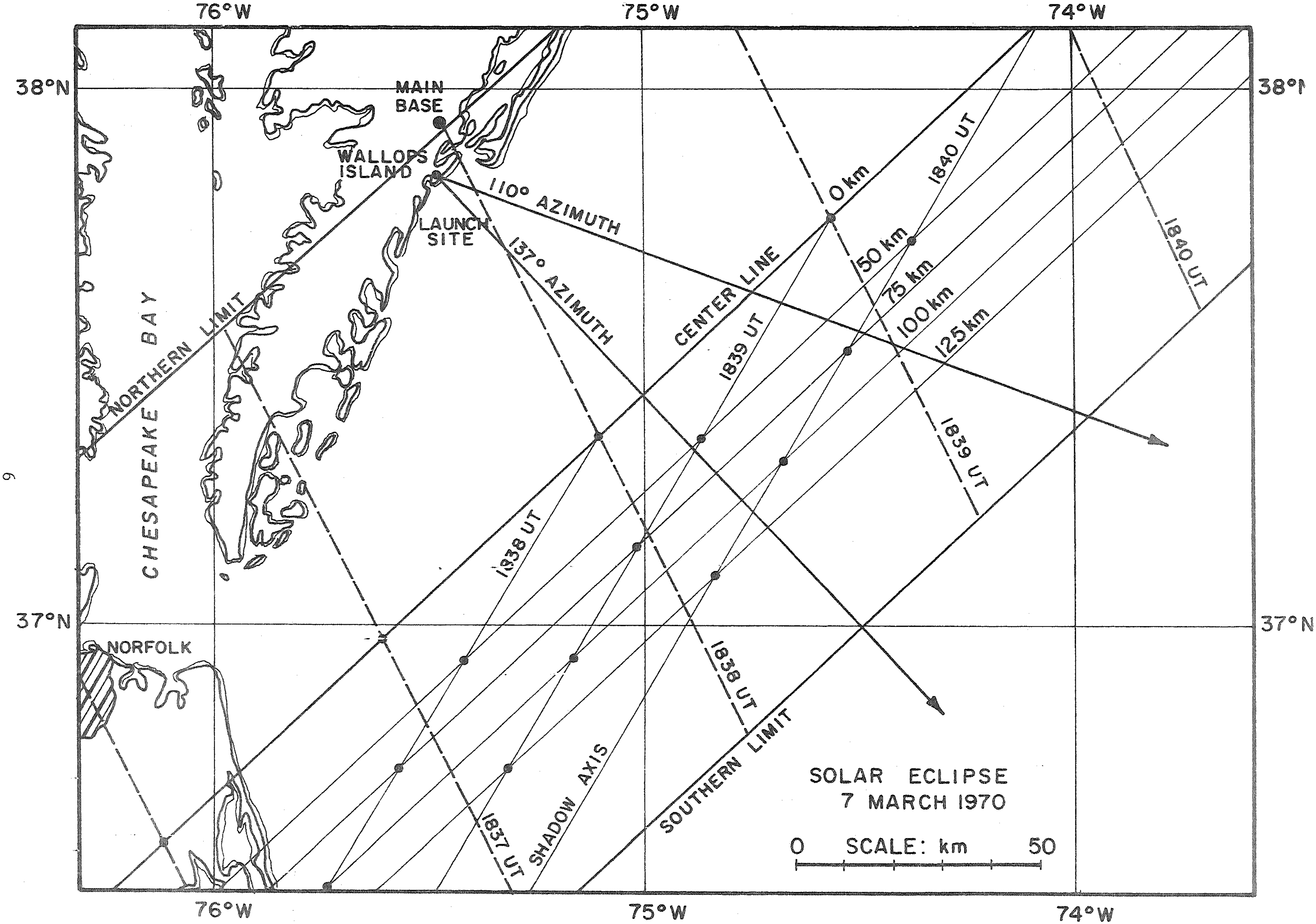

Figure 1. Path of totality in the vicinity of Wallops Island.

Data contained in the United States Naval Observatory Circular No. 125 have been used in plotting the eclipse path in Figure 1. The northern and southern limits and center line at ground level are shown. The smallest distance from the launch site to the center line is 61 km. The center lines at 50, 75, 100 and 125 km altitude are also shown. The eclipse at 100 km altitude is 30 km further, in horizontal range, from the launch site than at 0 km altitude. The time of mid-eclipse is indicated by the dashed lines nearly perpendicular to the eclipse path. The time of mid-eclipse at the launch site is 1837:53 UT. The corresponding times for the center lines at ionospheric altitudes can be estimated from the indicated positions of the shadow axis, as shown at 1838, 1839 and 1840 UT.

The velocity of the shadow is about 63 km/min (1.05 km/sec), moving, on an azimuth of 47°, to the northeast. The preferred rocket launch azimuth, indicated in Figure 1, is 137°, perpendicular to the center line.

The eclipse is perfectly located with respect to the launch site for E and F-regions studies but presents a problem for some D-region (60-90 km) investigations. Figure 2 shows the maximum duration of totality as a function of altitude and horizontal range from the launch site, on the preferred azimuth of 137°. The duration has a maximum possible value of 170 seconds on the center line and decreases to zero at the northern and southern limits. It is 74.6 seconds at the launch site.

Figure 2 also shows the trajectories of rockets having nominal launch elevation angles of 70°, 80°, 83° and 74.5°. The first three are actual

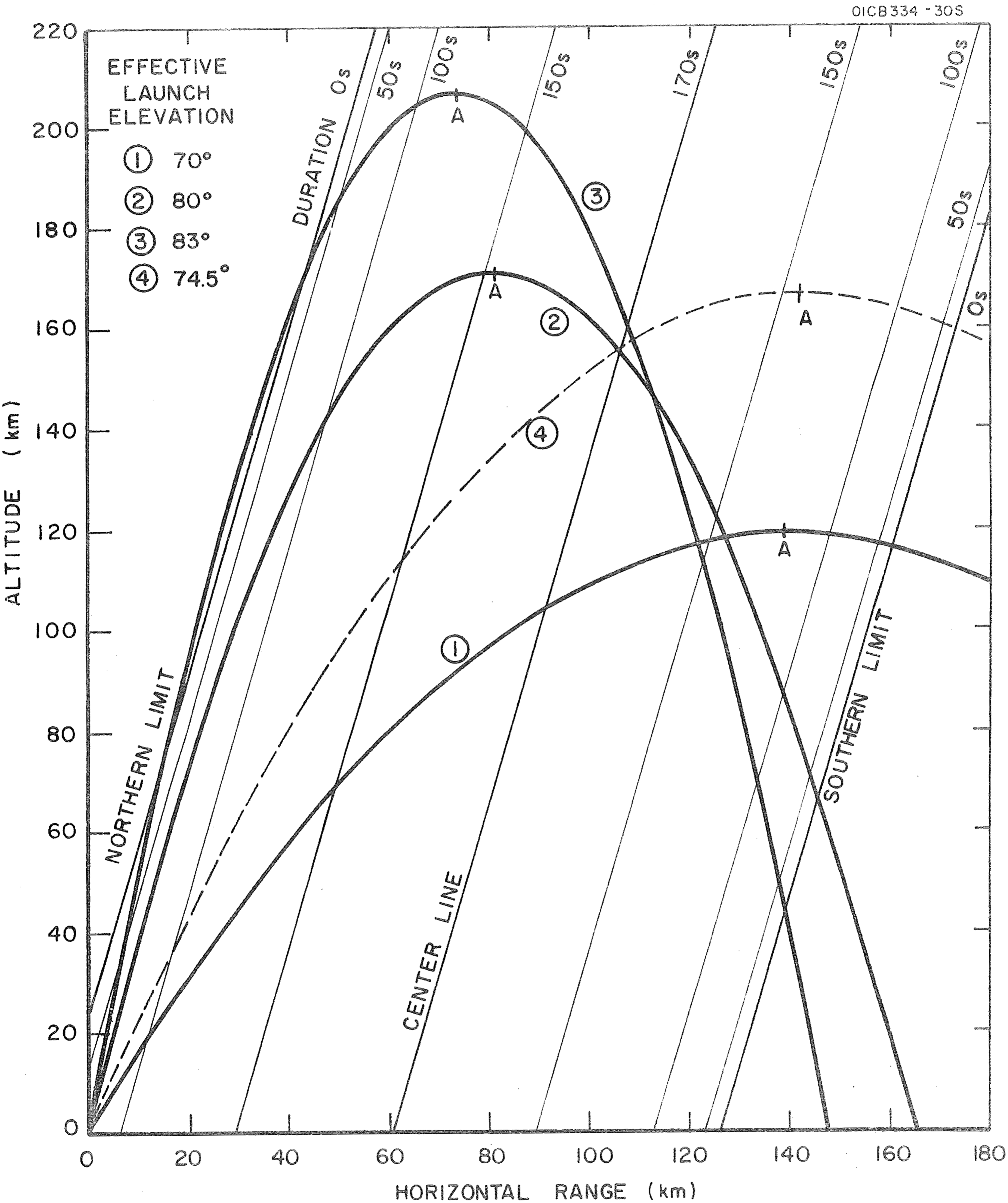

Figure 2. Maximum duration of totality for four rocket launch elevations.

values from the flights of Nike Apaches 14.147, 14.146, and 14.393, respectively. The fourth is the trajectory predicted for the eclipse rockets. The apogee point of each trajectory is indicated by the letter A.

The figure shows that with a high launch angle (83°) the rocket travels close to the northern limit to an altitude of about 180 km, and in the D-region, the eclipse duration is very short. For a moderate launch angle (80°), a much more favorable situation occurs in that a duration of 70 seconds is possible in the D region and still longer at greater altitudes. At 80 km, however, the rocket is only about 6 km inside the northern limit.

Decreasing the launch angle to a very low value (70°) places the rocket securely in totality in the D-region. There are several disadvantages, however. The aerodynamic heating of the payload is severe. The maximum altitude attained is considerably reduced. Also, the relatively low elevation of the line-of-sight from the launch site to the rocket is undesirable for the radio propagation experiment.

It appears from this discussion that a suitable trajectory would have a horizontal range of 40 km at an altitude of 80 km. Calculations performed by the Sounding Rocket Branch, NASA/GSFC, show that this will be accomplished with an effective launch angle of 74.5°. This predicted trajectory is the dashed curve in Figure 2. Table 3 shows the eclipse conditions for a rocket launched at 1837:10 UT on an azimuth of 135° and

TABLE 3

ECLIPSE CIRCUMSTANCES

Launch time 1837:10 UT; Launch Azimuth 135°; Launch elevation 74.5°

UT	Altitude(km)	T2(sec)	Duration(sec)	Disc(%)
1837:56.4	50.7	-2.49	105.8	0
1838:02.4	59.3	-2.42	111.5	0
1838:10.4	70.4	-2.42	119.4	0
1838:17.8	80.0	-2.87	126.3	0
1838:32.8	98.0	-4.59	139.3	0
1838:52.8	118.7	-8.62	153.3	0
1839:17.8	139.4	-16.0	167.3	0
1839:57.8	160.5	-31.3	173.1	0
1840:35.3	167.0	-44.8	151.9	0
1841:15.3	159.6	-28.5	41.0	0
1841:55.3	137.6	--	--	1.02
1842:15.3	121.1	--	--	1.93
1842:35.3	100.8	--	--	3.02
1842:55.3	76.8	--	--	4.24
1843:05.3	63.4	--	--	4.91
1843:15.3	49.0	--	--	5.61

with this predicted trajectory. The computer program used in this calculation is given as an appendix to this report. In Table 3 T2 is the time to second contact (i.e. start of totality) at the position of the rocket. Negative values mean that second contact has already occurred at that position and time. The duration of totality is also given, and, where the rocket is outside the region of totality the percentage of the area of the disc visible at the rocket is given. Where no figure is given for T2 or duration, that location was at no time in totality.

An interesting result of these calculations is that the vertical velocity of the rocket, by a remarkable coincidence, combines with the horizontal velocity of the inclined shadow axis to keep the rocket within a few seconds of second contact for the ascent through the D-region.

A final consideration, important for the solar radiation experiments, is the angular position of the sun in relation to the rocket trajectory. This determines the angles at which the detectors are mounted within the payload to ensue a nearly normal view of the sun during each revolution of the rocket.

The zenith and azimuth angles for the sun on 7 March 1970 are shown in Figure 3. At totality, these are 47° and 209°, respectively. With the rocket travelling on an azimuth of 135°, the angle between the rocket-sun direction and the rocket-spin axis is calculated to be 45°. This is easily obtained with the payload configuration shown in a subsequent section.

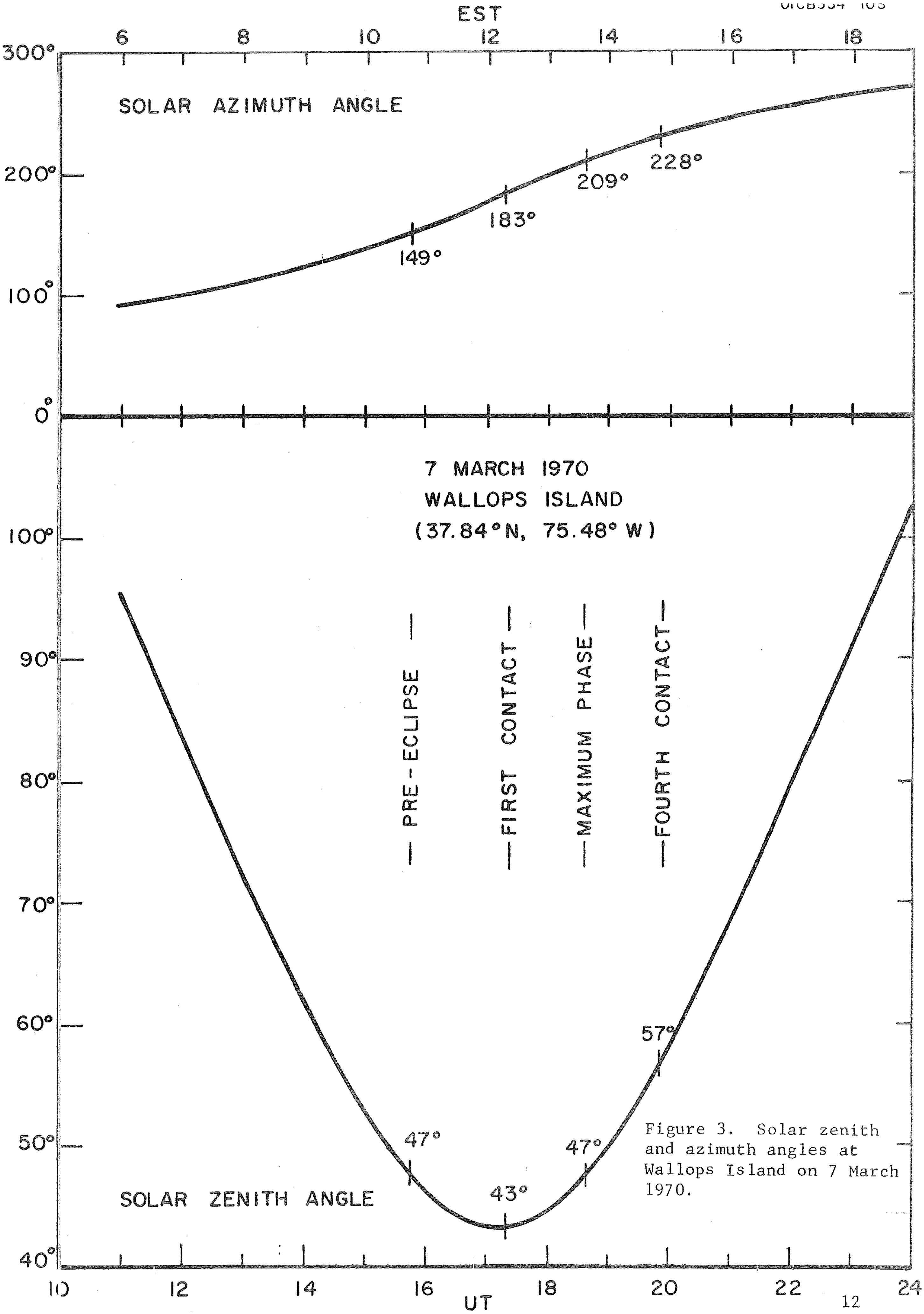

Figure 3. Solar zenith and azimuth angles at Wallops Island on 7 March 1970.

III. SCIENTIFIC OBJECTIVES

A. ELECTRON DENSITY

Data from the rocket launches during two previous solar eclipses have given a picture of the variation of electron density which is consistent with and extend data obtained from ground-based radio-propagation experiments. The two eclipses were those of 20 July 1963, observed from Fort Churchill, Manitoba, and of 12 November 1966, observed from Cassino, Brazil. In both cases, the sun was very quiet at the time of the eclipse.

The most striking finding, first noted in the 1963 eclipse(1) and subsequently confirmed in the 1966 eclipse,(2) is the large effect seen in the D-region below 75 km. The data of Figure 4 are profiles of probe current in the D and lower E-regions normalized to unity at 105 km. The area of solar disc visible at the rocket position is 8 percent for profile 1, 15 percent for profile 2, 60 percent for profile 3 and 98 percent for profile 4.

The data of Figure 5 combine the probe and propagation experiments to give absolute values of electron density. Curve 1 was obtained before totality with 3 percent of the disc visible. Curve 2 gives the profile at second contact (at 80 km). Curve 3 gives the profile at third contact (at 80 km). Curve 4 gives the profile for full sun, after the eclipse. These data demonstrate a remarkable and unexpected decrease in electron density even during totality.

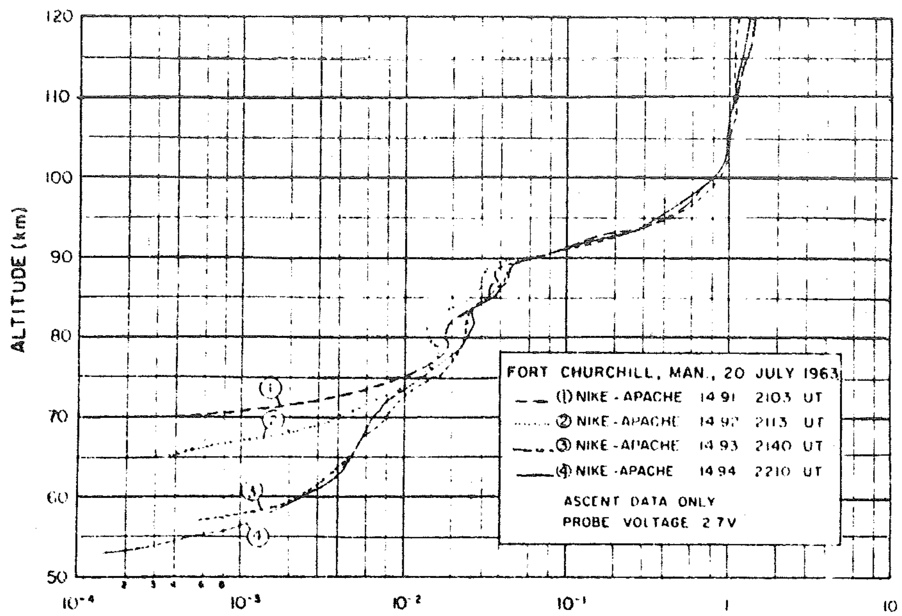

Figure 4. Profiles of probe current in the D- and lower E-regions, normalized to unity at 105 km.

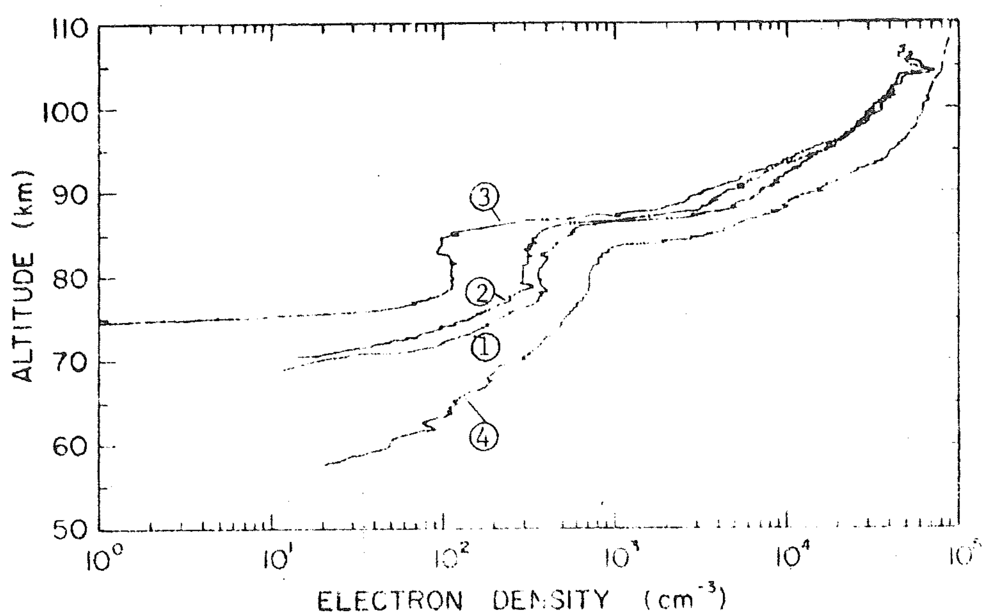

Figure 5. Profiles of electron density during and following the eclipse of 12 November 1966.

Theoretical analysis by Keneshea and Fowler,[3] following the revelations of the Churchill eclipse observations, have obtained rather good agreement with the rocket observations. Their calculations of electron density profiles for the Brazil eclipse are shown in Figure 6.

One major objective of the proposed eclipse series is to determine whether, in fact, the lowest electron densities occur at the end of totality. Because of the role of ozone in D-region ion chemistry and the expected delay in maximum ozone concentration beyond totality it is possible that the minimum electron density, at say 80 km, is delayed and occurs shortly after totality. A measurement of electron density (and ozone, see below) will be made about two minutes after third contact.

B. ELECTRON TEMPERATURE

The relation between electron temperature and the neutral gas temperature was first considered in detail by Hanson and Johnson.[4] They found that, under steady-state conditions the temperature difference between electrons and the neutral gas should be negligible below 150 km and above 300 km. Nonequilibrium was predicted for the intervening region, the temperature of the thermal electrons being greater than that of the neutral gas by as much as 50 percent. Subsequent analysis of Dalgarno, et al.[5] using improved information on absorption cross sections for the atmospheric gases and further refining the calculations by considering, for example, thermal conduction show that nonequilibrium can be expected at altitudes above 120 km.

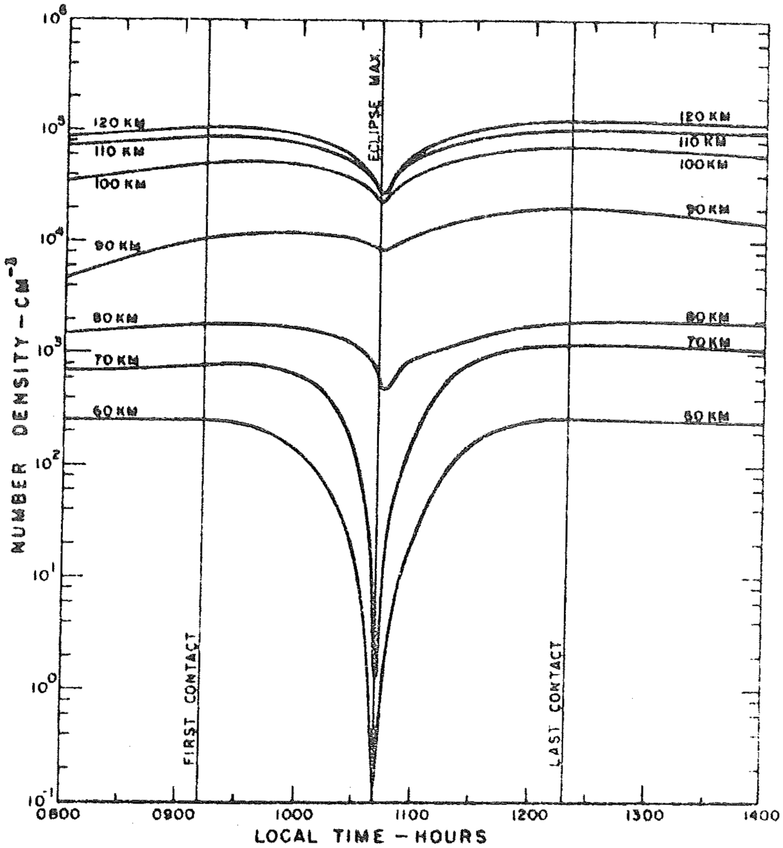

Figure 6. Electron density vs altitude for the eclipse of 12 November 1966 at Cassino, Brazil.

Rocket observations[6] confirm the absence of thermal equilibrium in the E-region and there is evidence that the difference in termperature of electrons and neutral gas increases with increasing sunspot number.

Observations of electron temperature during two eclipses[1,6] show that the electron temperature in the E-region does not change during an eclipse whereas, at greater altitudes, a change is detected. The data from the eclipse of 12 November 1966 are shown in Figure 7. The difference in electron temperature between a rocket flight after the eclipse (14.303:1600 UT) and two flights in mid-eclipse (14.303:1406 UT and 14.304:1410 UT) is plotted as a function of altitude. Some data from one flight are missing. Below 150 km the electron temperature is constant within the experimental error ($\pm$ 25°K in each observation); above 150 km a nearly linear change with altitude is found amounting to 300°K at 190 km.

The eclipse data on electron temperature appear to show the absence of direct control by solar radiation at altitudes below 150 km, as predicted by Hanson and Johnson.[4] It should be noted, however, that the electron temperature in the upper E-region was several hundred degrees greater than the neutral gas temperature.

C. NEUTRAL COMPOSITION

It is not expected that the atmospheric density changes during the eclipse to an extent that is detectable with present techniques. It is proposed to measure the concentration of O_2 shortly before the eclipse

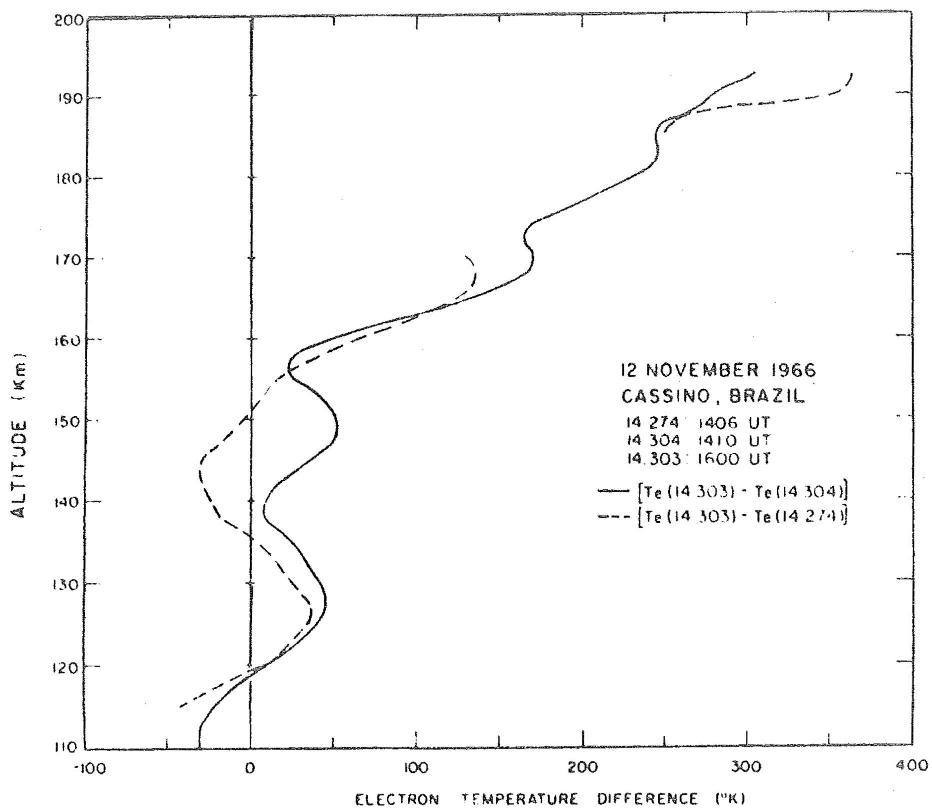

Figure 7. The change in electron temperature observed during the solar eclipse of 12 November 1966. Some data from Nike Apache 14.274 are missing.

as a reference. The method of measurement,[7] from the extinction profile of Lyman-α (1216Å) radiation gives the O_2 concentration between 65 and 95 km. The Lyman-α detector will be included in the payloads near totality for determining the incident flux; it is not expected that an extinction profile will be determined on these flights.

A Geiger counter sensitive to the range 44 to 60Å will be included in the payload. This radiation is absorbed in the height range of about 95 to 115 km. However, as shown in Figure 8,[1] the large statistical errors associated with the relatively low count rate of this detector limit the accuracy for density determination to a small height interval centered on unit optical depth. The primary reason for including this detector is for determination of the incident flux, i.e., at altitudes above about 120 km, as discussed in a later section.

The role of the minor neutral constituents in the chemistry of the D-region makes it important to obtain as much information as possible about their variation during the eclipse. Calculations by Hunt,[8] Figure 9, and by Keneshea and Fowler,[3] Figure 10, indicate a marked increase in ozone during the eclipse with the maximum occurring about 10 minutes after maximum phase.

The overall plan of the series of launches limits the ozone measurement to one profile at about 2 minutes after totality and another prior to the eclipse.

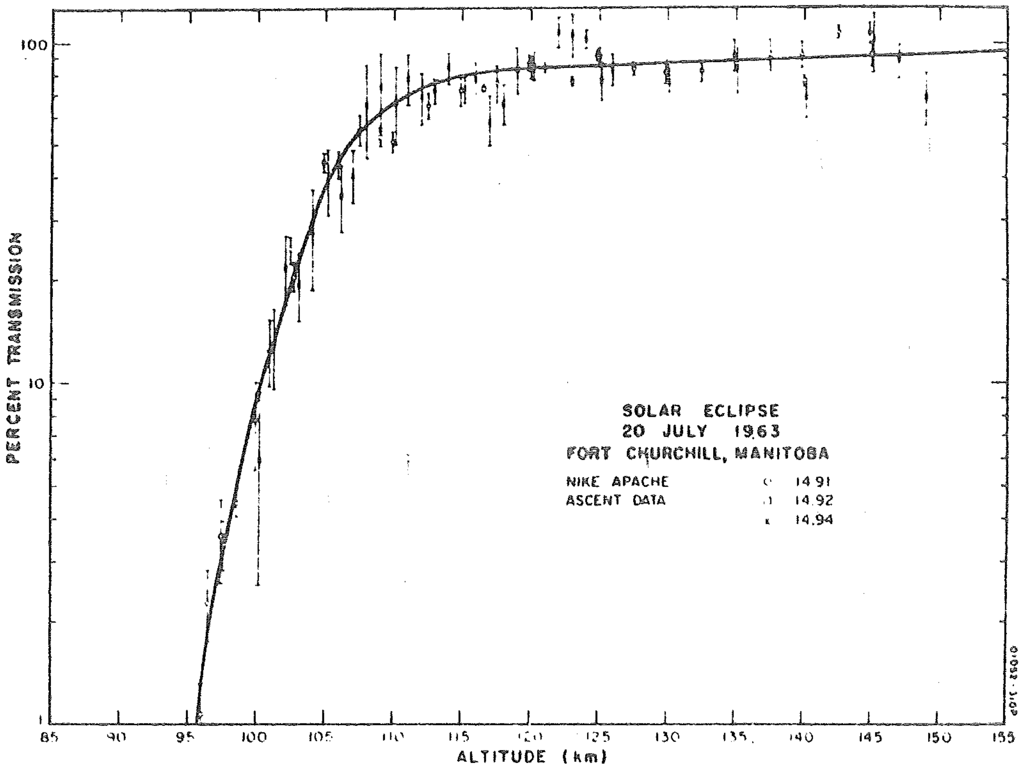

Figure 8. Absorption profiles of X-rays (44-60Å).

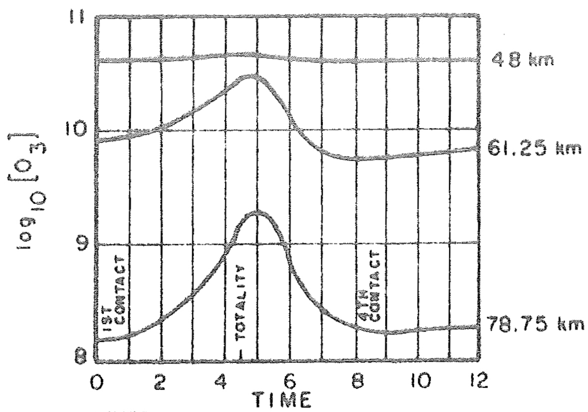

Figure 9. The variation of the ozone concentration at various altitudes during an eclipse. Time is expressed as thousands of seconds after noon.

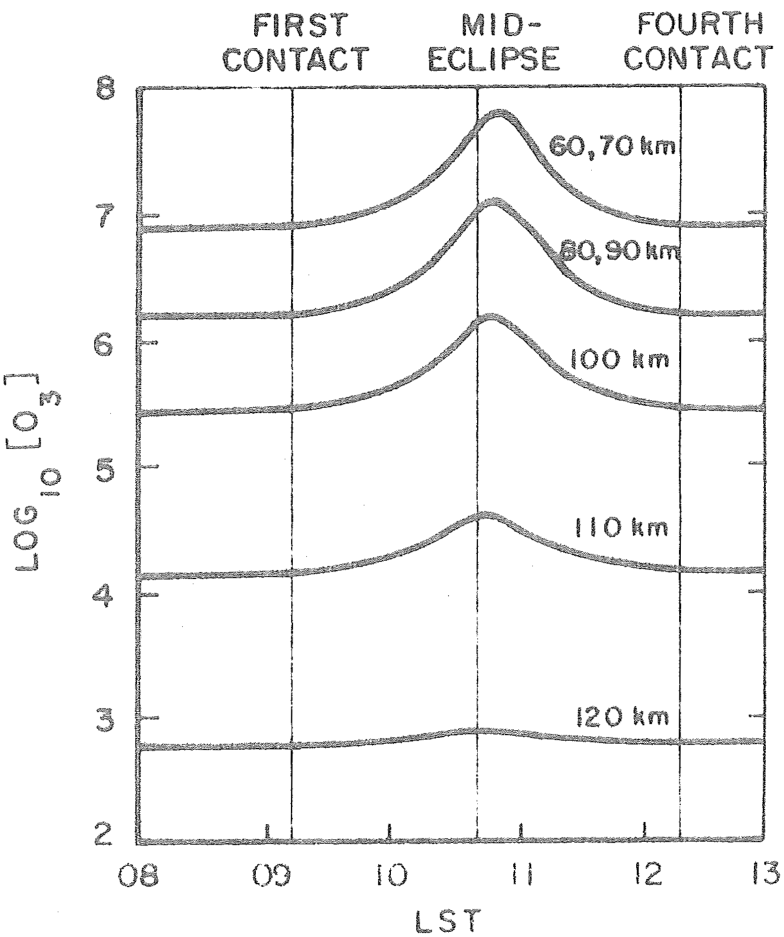

Figure 10. Variation of ozone concentration computed for the eclipse of 12 November 1966, Cassino, Brazil.

The normal daytime ozone concentration can be determined to an altitude of 70 km under the most favorable conditions (mainly involving vehicle motion). The calculations of Keneshea and Fowler shown in Figure 10 imply that, near totality, the profile can be extended to 90 km.

It will not be possible to demonstrate the delay in ozone maximum and it is hoped that other experimenters will be able to investigate this point. It is also hoped that other observations of neutral and charged species will be available from mass spectrometer experiments in this same eclipse.

D. SOLAR RADIATION

The observation of the flux of solar radiation above the absorbing region of the atmosphere is important in two ways. The first concerns their interaction with the atmosphere in interpretation of the observations discussed previously, particularly electron density, electron temperature and ozone concentration. The second concerns the source of these radiations on the sun. As noted previously, the absorption profile of each radiation gives some information on the concentration of neutral species or total density (in the case of X-radiation).

It is proposed to include detectors to measure solar flux at three wavelengths representing coronal, chromospheric and photospheric radiation. These are, respectively, soft X-rays (44-60Å), Lyman-α (1216Å) and 2600Å. In addition, calibration of the solar aspect sensor will give additional information in the visible part of the solar spectrum. Several very interesting observations are possible with this relatively simple instrumentation on a sounding rocket.

The E layer, at about 110 km, being the most regular of the ionospheric layers, shows a clearly defined eclipse effect. The electron density decreases as the sun's disc is gradually obscured, but even in total eclipses of the maximum possible duration (about 7 minutes), the electron density never decreases to less than one third of its normal value. This effect was initially ascribed to the "sluggishness" of the ionosphere. However, this required a rather low value of recombination coefficient (2×10^{-8} cm^3 sec^{-1}) and would also require that the minimum electron density was about 5 minutes delayed beyond the end of totality. This value of recombination coefficient is unacceptable; recent laboratory and theoretical studies indicate a value larger by an order of magnitude. Also, the time lag is not always present, and on some occasions is negative (i.e., the minimum electron density precedes totality).

An alternative, and currently the most acceptable explanation, is that the source of ionizing radiation is coronal and is, therefore, not reduced to zero during a total eclipse. Figure 11 shows a model used by Keneshea and Fowler[(3)] based on a study by Elwert.[(9)] This is supported by rocket observations[(1)] which show a significant fraction (about 20 percent) of the solar X-rays (44-60Å) flux is present at totality. It is planned to repeat this observation and to extend it by observing the detailed variation of flux at two times during totality and subsequently, about two minutes after totality. In addition, the unobscured flux will be determined on the pre-eclipse flight.

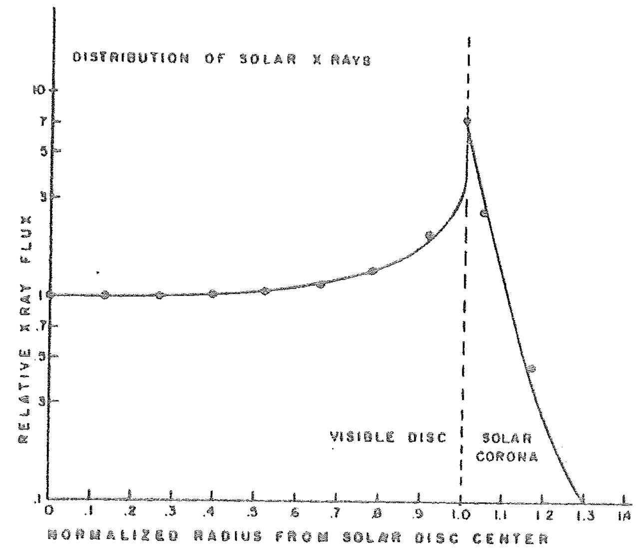

Figure 11. Solar X-ray spatial distribution assumed in the model.

Lyman-α radiation is important in the formation of the normal D-layer at about 80 km. This source of this radiation is the chromosphere, about 5,000 km thick above the photosphere (visible disc). The eclipse is thus of smaller magnitude for Lyman-α than for visible radiations. This is illustrated in Figure 12 for the eclipse of 12 November 1966. The data refer to the actual trajectory of Nike Apache 14.274. The curves show the calculated percentage of the disc visible at the position of the rocket. That labelled $\alpha = 0$ refers to the visible disc, i.e., the eclipse as seen in the visible part of the spectrum. The curves labelled $\alpha = 0.01$ and $\alpha = 0.02$ refer to larger disc size by 1 and 2 percent, respectively. The crosses show the observed flux of Lyman-α as a percentage of that of the unobscured sun. It is seen that the chromosphere has a diameter about 0.5 percent larger than the visible disc, in agreement with present knowledge of the sun.

The Lyman-α data are limited to the time the rocket is above the absorbing region. The data from the launches in the eclipse of 7 March 1970 will be superior in that the timing is such that the actual exit from totality for Lyman-α will be observed well above the absorbing region.

A similar experiment will be performed for the 2600Å radiation. This should show the same variation as the visible part of the spectrum. It will be possible to examine these data for evidence of limb darkening such as is observed for visible radiation.

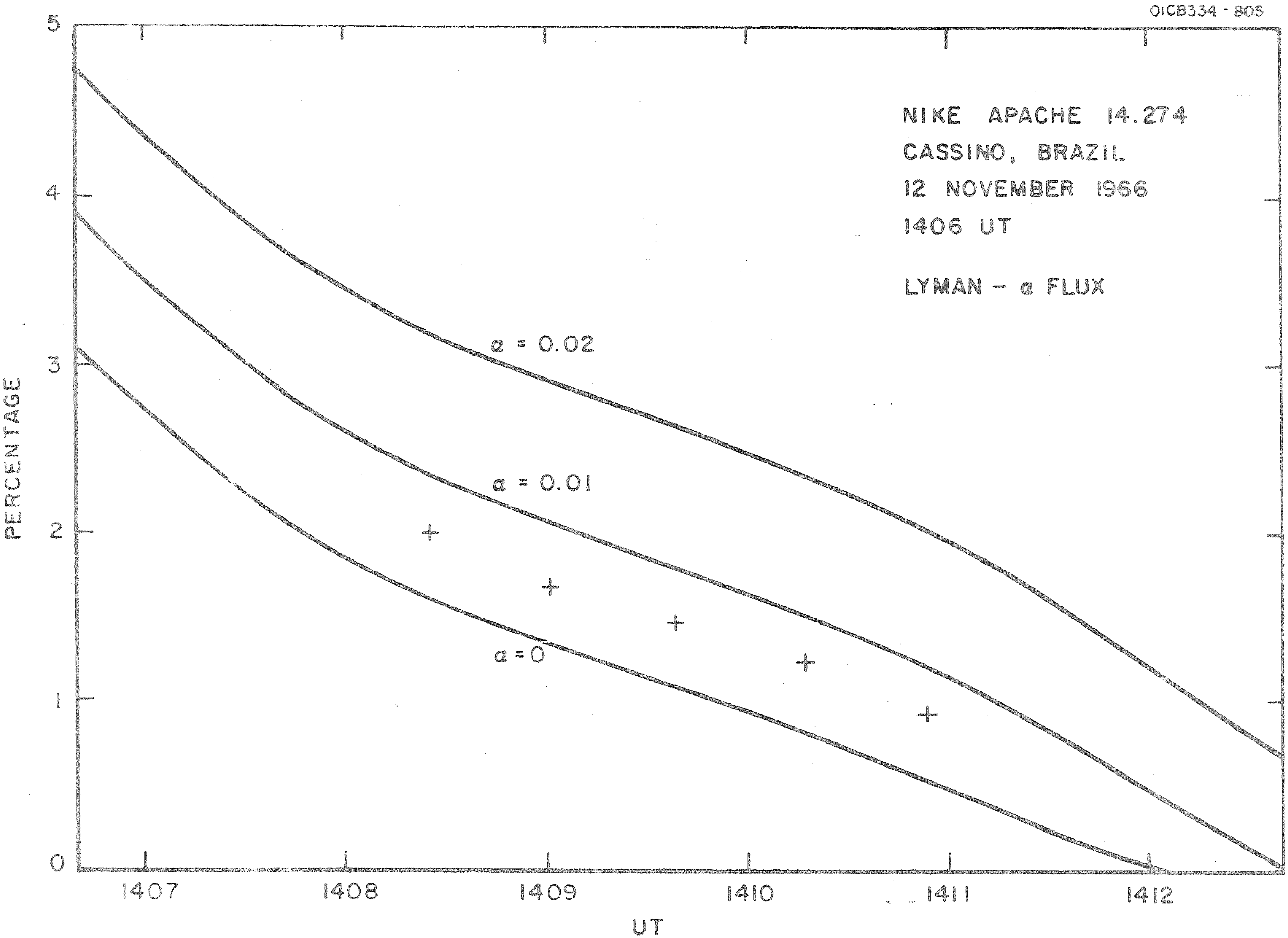

Figure 12. Lyman-α flux observed during the eclipse of 12 November 1966.

IV. ROCKET INSTRUMENTATION

Five payloads for Nike Apache rockets have been constructed for the eclipse launches. For maximum economy and flexibility in this operation, the payloads will be almost identical, differing in details of sensor orientation and sensitivity.

The new payload design is derived from the basic type, designated Type A, first flown in April 1964 on Nike Apache 14.143. It consists of a DC/Langmuir probe experiment, a CW propagation experiment and solar radiation experiments together with magnetic and solar aspect sensors and telemetry, power and control systems. The solar radiation detectors are protected by doors up to an altitude of 50 km.

The payload for the proposed eclipse launches is designated Type A Mod. 7. The major redesign is in the portion containing the solar radiation detectors and solar aspect sensor. In order to include an additional detector, it is planned to replace the single deck arrangement of previous payloads with two separate decks, as shown in Figure 13. One deck carries two UV detectors (Lyman-α and 2600Å) and their associated circuits. The second deck contains the solar aspect sensor and the solar X-ray detector (44-60Å) together with their circuits, which, as discussed below, are interrelated. The X-ray detector has not previously been included in the Type A payload but has been used previously in experiments on other programs, including the successful series at Fort Churchill during the eclipse of 20 July 1963.

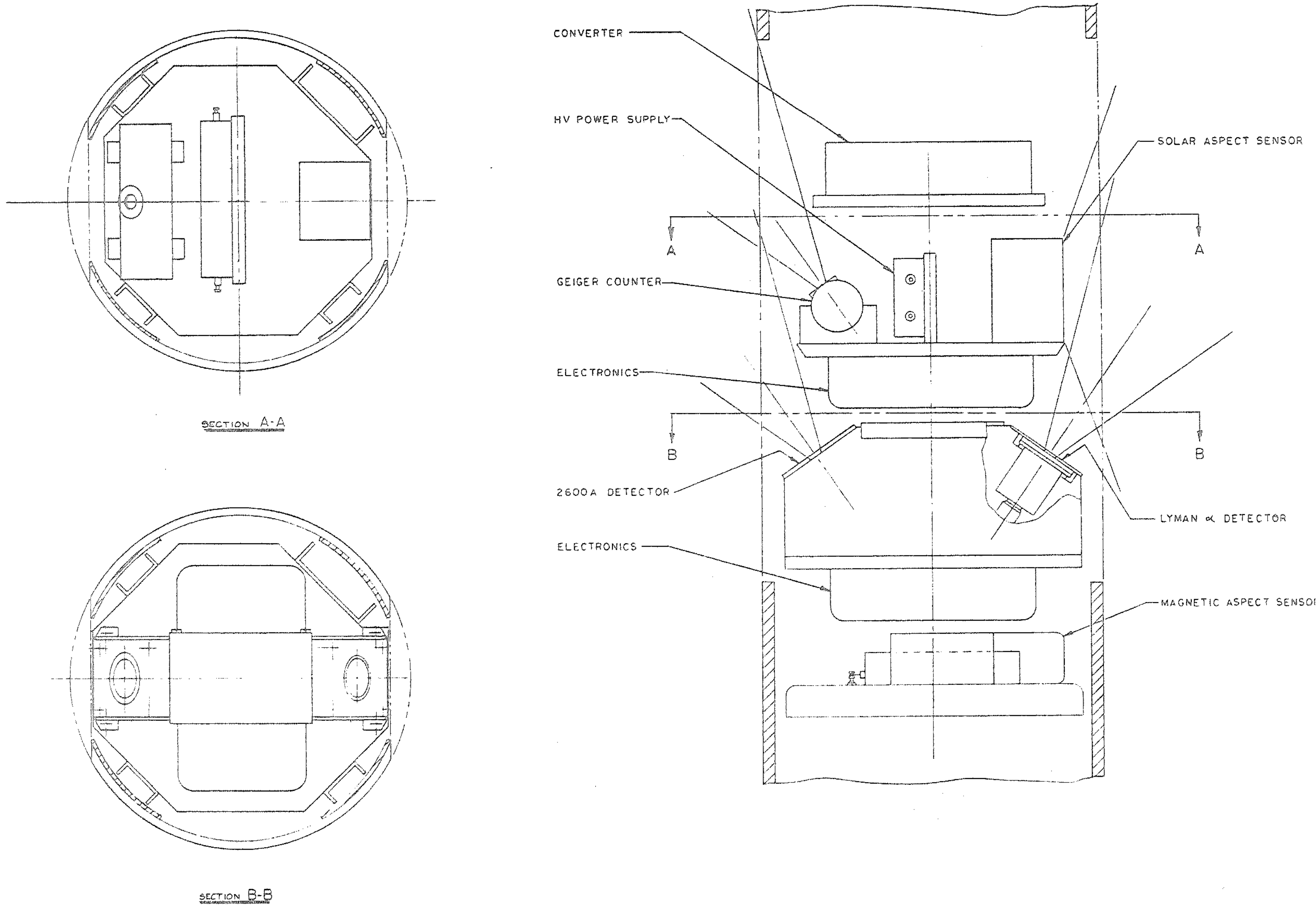

Figure 13. The configuration of the solar radiation experiment.

The detector for X-rays in the wavelength band 44-60Å uses a window of mylar, thickness 1/4 mil (6×10^{-4} cm) and is filled with neon at a pressure of 1/2 atmosphere to which is added 1 percent isobutane as a quenching agent. The diameter of the window for the pre-eclipse measurement (i.e. full sun) is set at 20 mil (5×10^{-2} cm), corresponding to an expected flux of the order of 0.1 erg cm^{-2} sec^{-1}. For the measurements in and near totality the diameter is chosen as 50 mil (1.3×10^{-1} cm). These values are not critical because of the large dynamic range inherent in the use of a Geiger counter.

The output signal from the Geiger counter is made suitable for presentation on a 0 to 5 volt scale at the input of the SCO using the circuit indicated in Figure 14. The output pulses of the Geiger counter, developed across the 1 meg resistor in series with the high voltage (1kV) power supply, have typically a 5 microsecond rise time, and a 25 microsecond decay to 50 percent of their peak amplitude. The amplitude is variable up to a value of a few volts.

Each pulse is amplified in the charge amplifier and if it exceeds a pre-set threshold level, it triggers a one-shot multivibrator whose output is a pulse of fixed amplitude (5V) and duration (50 μsec). A staircase generator is used as a digital to analog converter. It consists of a scale of 32 combined with an adding circuit. The circuits are arranged such that each pulse produces an increment of voltage of 5/32 volt at the output. When the output reaches 5 volts the scale of 32 resets the output to 0 volts. Thus, each return to zero represents

01B405-10 E

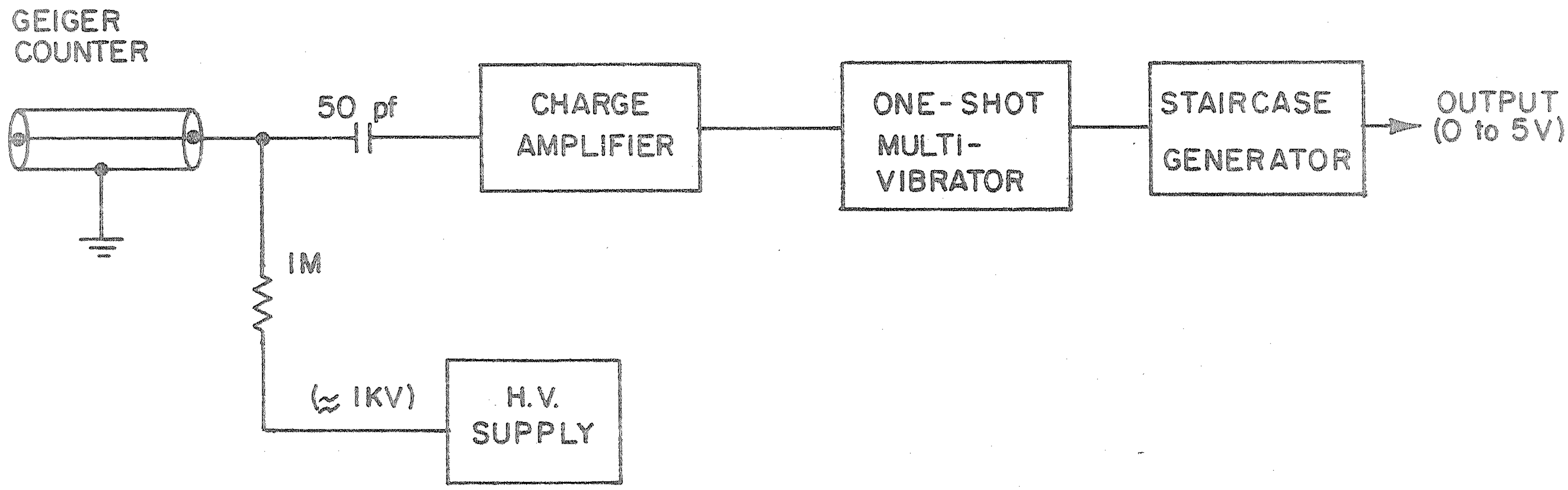

Figure 14. Geiger Counter Circuit

32 counts and yet single pulses can be easily counted. This relatively simple circuit is appropriate to the data reduction from paper records.

The output from the X-ray experiment is combined with that of the solar aspect sensor on channel 19 of the telemetry system. A simple electronic switch is used to give a total period of 0.6 sec divided equally between the two signals. This value is chosen on the basis of an expected spin rate of 6 rps.

The circuits of the other experiments are unchanged from those used in previous flights. The interconnection wiring diagram of the payload is shown in Figure 15.

The telemetry system uses an FM/FM transmitter (Dorsett Model 501B) having a power output of 1.2 watts. The assignments of the ten data channels is given in Table 4. As noted there, the frequencies used in the propagation experiment are 2225 kHz and 3385 kHz.

The configuration of the payload is shown in Figure 16. The overall length is 73.6 inches and the weight is 59 pounds. A radar transponder (S-band), provided by Wallops Island, will be mounted between the payload and the second-stage motor (Apache) bringing the total effective payload weight to about 65 lbs.

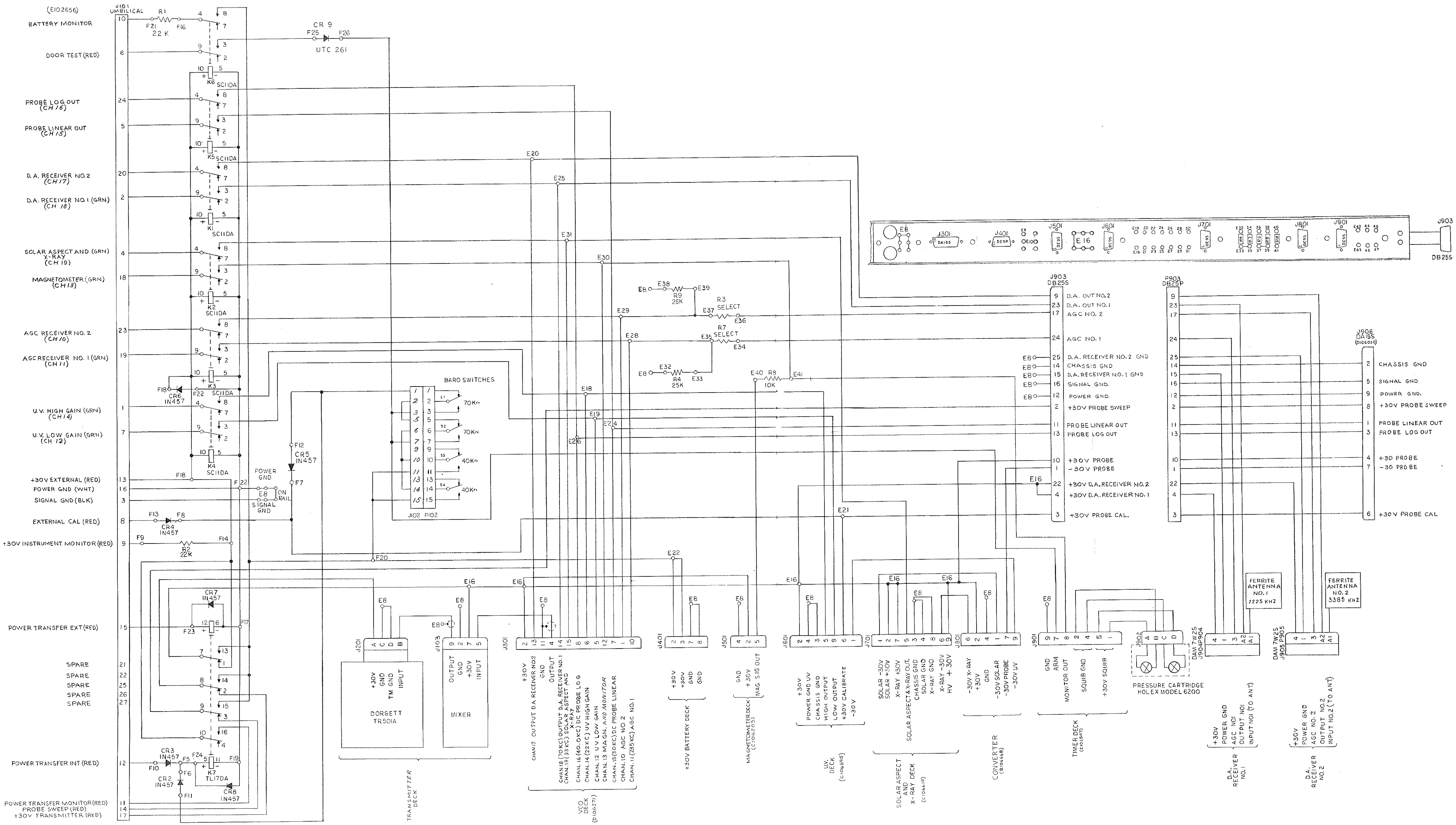

UNLESS OTHERWISE SPECIFIED ALL DIM ARE IN INCHES. TOLERANCES .X ± .05 .XX ± .02 .XXX ± .005 ANGLES MACHINE FINISH ✓ BREAK SHARP EDGES AND COR .005 TO .020R APPROX	DR L. Johnson DATE	GCA TECHNOLOGY DIVISION Bedford, Massachusetts	
MATERIAL	CHK / APPROVALS / RELEASED / FINAL FINISH	TITLE INTERCONNECTION WIRING PAYLOAD A MODEL 7	
NEXT ASSY / USED ON / APPLICATION		SIZE R	DRAWING NO. 106594
		SCALE NONE	WT / SHEET 1 OF 1 / REV 0

DO NOT SCALE

TABLE 4

TYPE A MOD. 7: TELEMETRY CHANNEL ASSIGNMENTS

Ch. 19	Solar Aspect and X-ray Detector
Ch. 18	Receiver #1 (2225 MHz), modulation
Ch. 17	Receiver #2 (3385 MHz), modulation
Ch. 16	Probe, Log
Ch. 15	Probe, Linear
Ch. 14	UV, High Gain
Ch. 13	Magnetic Aspect and Door Release Monitor
Ch. 12	UV, Low Gain
Ch. 11	Receiver #1, AGC
Ch. 10	Receiver #2, AGC

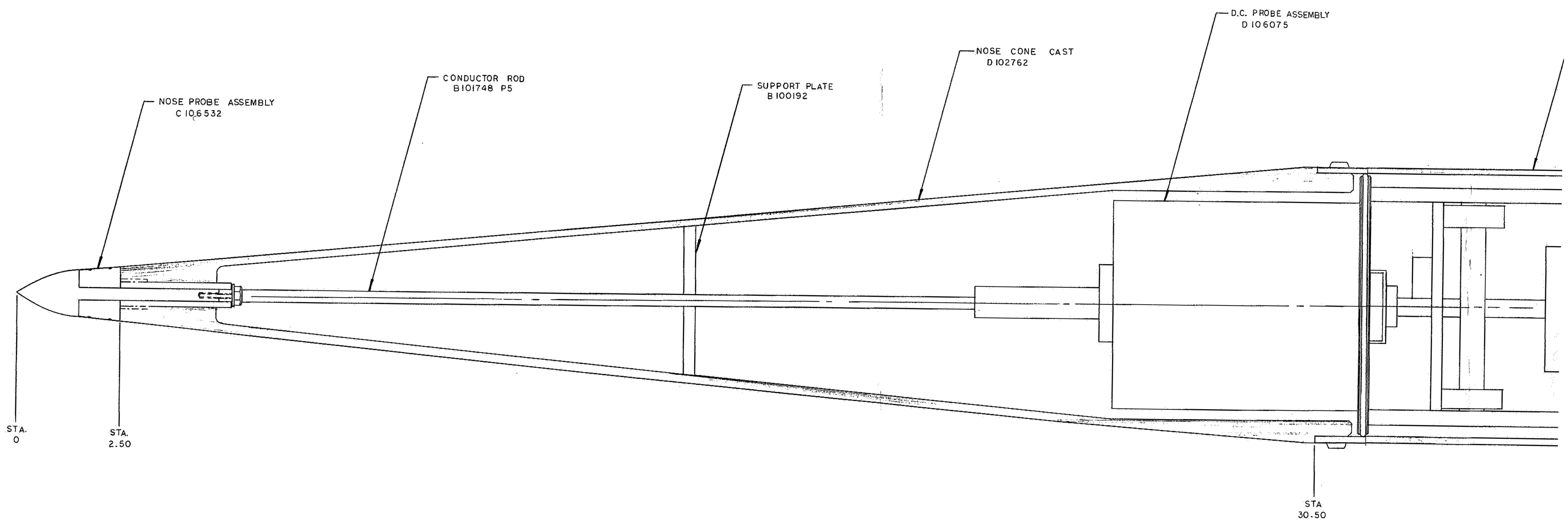

NOSE PROBE ASSEMBLY
C 106532
CONDUCTOR ROD
B101748 P5
SUPPORT PLATE
B100192
NOSE CONE CAST
D102762
D.C. PROBE ASSEMBLY
D 106075
STA.
0
STA.
2.50
STA
30.50

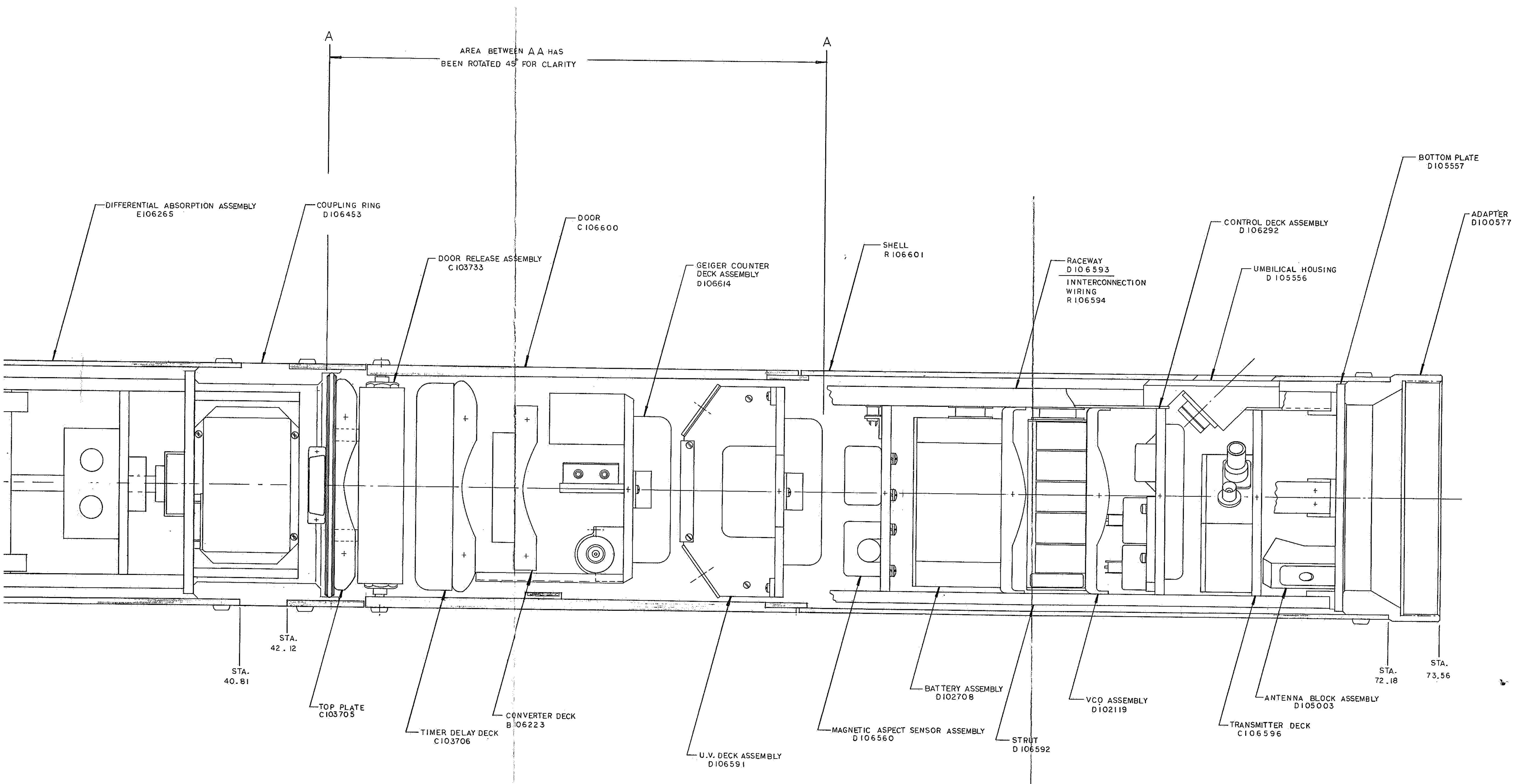

UNLESS OTHERWISE SPECIFIED ALL DIM. ARE IN INCHES TOLERANCES .X±.06 .XX±.02 .XXX±.005 ANGLES MACHINE FINISH ✓ BREAK SHARP EDGES AND COR. .005 TO .020R APPROX	DR / DATE CHK APPROVALS RELEASED	GCA TECHNOLOGY DIVISION Bedford, Massachusetts GCA CORPORATION
MATERIAL	FINAL FINISH	TITLE PAYLOAD ASSEMBLY TYPE A M.O.D. 7
NEXT ASSY: 1-318	USED ON	SIZE R — DRAWING NO. 106599
APPLICATION		SCALE 1:1 — WT — SHEET 1 OF 1 — REV 8

DO NOT SCALE

7

V. FIELD OPERATIONS

The eclipse occurs on the afternoon of Saturday, 7 March 1970. Maximum phase (mid-totality) at the Wallops Island launch site occurs at 1837:53 UT (1337:53 EST). The first rocket (Nike Apache 14.435) is to be launched at 1545 UT (1045 EST), about 90 minutes before first contact. For this flight the launch azimuth will be 110°, and the launch elevation will be 78°. The following three launches will occur during and immediately following totality.

The launch times have been determined on the basis of the following criteria:

Nike Apache 14.436. This rocket is to arrive at an altitude of 80 km at second contact.

Nike Apache 14.437. This rocket is to follow the preceding rocket after an interval of 50 seconds and also to be within totality at an altitude of 80 km.

Nike Apache 14.438. This rocket is to arrive at an altitude of 80 km after totality with 1.5 percent of the solar disc visible from the position of the rocket.

The launch times calculated using the predicted trajectory for a launch azimuth of 135° and a launch elevation of 74.5° are given in Table 5. Nike Apache 14.439 is a back-up to be launched only in the event of a catastrophic failure of vehicle or telemetry within 30 seconds after launch of any of the preceding three rockets.

TABLE 5

ECLIPSE LAUNCHES

Nike Apache	Time(UT)	Azimuth(deg.)
14.435	1545:00	110
14.436	1837:10	135
14.437	1838:00	135
14.438	1840:40	135
14.439	Back-up	135

Each payload will radiate on a separate frequency, none of which will be used on any other part of the Wallops Island operation taking place on the same day.

The payloads use a "fly away" umbilical connector, i.e. one which automatically disengages with first motion of the rocket. All five umbilical cables will be terminated in the GCA payload control console. The rapid sequence of launches will be handled from the console arrangement shown in Figure 17. Each umbilical cable contains two sets of wires; one set is used for control functions and the other for monitoring functions. The wires for the control functions are brought to individual switches on the launch console. The wires for the monitor functions are brought to rotary switches. Each payload, in turn, can be selected and the various functions observed on meters and on the oscilloscope. In this way, using a minimum of components, great operational flexibility is obtained.

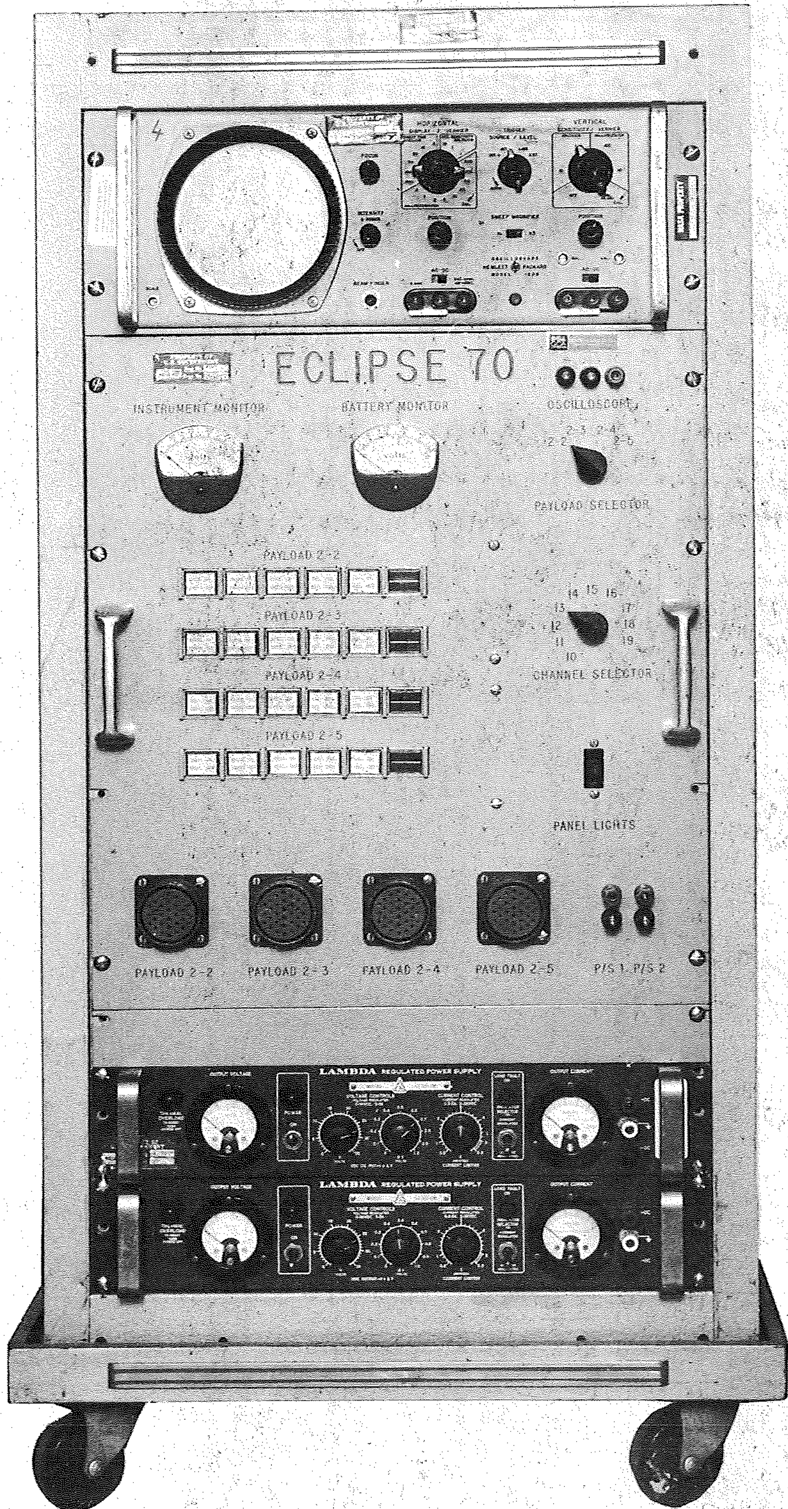

Figure 17. Payload Control Console for the Eclipse Operation

VI. FUTURE PLANS

Activities for the month of February 1970 will be almost entirely devoted to final preparations for the series of launches scheduled for the eclipse of 7 March 1970. The five payloads have, during January 1970, been subjected to telemetry integration and environmental tests at Goddard Space Flight Center. During the first two weeks of February 1970 the final testing and calibration of the experiments will be performed. The last two weeks of this month and the first week of March will be spent at Wallops Island making final preparations for the eclipse operation. The schedule at Wallops Island in this period includes rehersal of the launch operations and final tests of the payload.

Longer range plans on this program include an investigation of intense Sporadic-E. Preparation of a payload, which will include a measurement of electric field, will be started following the completion of the eclipse operation. A launch in July 1970 is planned. Concurrently with the work on the Sporadic-E experiments the reduction and analysis of data from the eclipse flights will be undertaken.

REFERENCES

1. Smith, L. G., et al., J. Atmos. Terr. Phys. 27, 803,(1965).

2. Mechtly, E. A., et al., Radio Sci. 4, 371, (1969).

3. Keneshea, T. J., and R. J. Fowler, AFCRL Report 66-741, (1966).

4. Hanson, W. B., and F. S. Johnson, Mem. Soc. Roy. Sci. Liege, 4, 390, (1961).

5. Dalgarno, A., et al., Planet. Space Sci. 15, 331, (1967).

6. Smith, L. G., et al., J. Atmos. Terr. Phys. 30, 1301, (1968).

7. Weeks, L. H., and L. G. Smith, J. Geophys. Res. 15, 4835, (1968).

8. Hunt, B. G., Tellus 17, 516, (1965).

9. Elwert, G., J. Atmos. Terr. Phys. 12, 187, (1958).

APPENDIX

Computer Program for the Eclipse of 7 March 1970

A computer program designed primarily for use with a rocket trajectory has been prepared to calculate the circumstances of the 7 March 1970 total solar eclipse. The equations for the program are found in the Explanatory Supplement to the Ephemeris, 1961. The Besselian elements contained in the program are tabulated in the American Ephemeris and Nautical Almanac, 1970. These are reproduced in Table 1. The values for 1830 ephemeris time are used in the program.

The program has been verified using data from the US Naval Observatory Circular No. 125. An example of the input and output data format is attached.

This program was developed by R. V. Sillars, with modifications by L. G. Smith and G. A. Pintal.

```
01000*    ECLIPSE OF 7 MARCH 1970
01005 PROGRAM ECLIP2
01007*  REFERENCE 1830UT
01010 PI=3.1415927
01020 SX=60.0
01030 DR=0.017453293
01040 F2=0.99327733
01050 U0=94.72688*DR
01060 D0=ATAN(-0.091063/0.995845)
01070 TF1=0.004710
01080 TF2=0.004687
01090 DUM=0.261865
01100 DD=0.000271
01110 1 READ 99
01120 PUNCH 99
01130 PUNCH 90
01140 PUNCH 90
01150 READ 94,M
01151 TH=18.0
01152 TM0=30.0
01154 X0=0.220318
01156 X1=0.304554
01158 Y0=0.628851
01160 Y1=0.674683
01162 EL10=0.539479
01164 DEL1=0.000008
01166 EL20=-0.006832
01168 DEL2=0.000007
01170↑DX=(X1-X0)*6.0
01180↑DY=(Y1-Y0)*6.0
01190↑DO 50 J=1,M
01200 READ 93,TM,TS,ALT,FLONG,FLAT
01210
01220↑SPHI=SIN(FLAT*DR)
01230↑CPHI=COS(FLAT*DR)
01240↑Q=SQRT(1.0/(CPHI**2+F2*(SPHI**2)))
01250↑PS=(F2*Q+0.15677940E-03*ALT)*SPHI
01260↑PC=(Q+0.15677940E-03*ALT)*CPHI
01270 TN=TM+TS/SX+0.645
01280↑TE=TH+TN/SX
01290↑X=X0+(DX/SX)*(TN-TM0)
01300↑Y=Y0+(DY/SX)*(TN-TM0)
01310↑EL1=EL10+0.1*DEL1*(TN-TM0)
01320↑EL2=EL20+0.1*DEL2*(TN-TM0)
01330 D=D0+DD*(TE-18.5)
01340↑SD=SIN(D)
01350↑CD=COS(D)
01360 UM=U0+DUM*(TE-18.5)
01370 HH=UM-FLONG*DR-0.00281435
01380↑SH=SIN(HH)
01390↑CH=COS(HH)
01400↑XI=PC*SH
01410↑ETA=PS*CD-PC*SD*CH
01420↑ZET=PS*SD+PC*CD*CH
01430↑DXI=DUM*PC*CH
01440↑DETA=DUM*XI*SD-ZET*DD
```

```
U=X-XI
DU=DX-DXI
V=Y-ETA
DV=DY-DETA
EN2=DU**2+DV**2
EN=SQRT(EN2)
DEL=(U*DV-DU*V)/EN
DDD=U*DU+V*DV
ELL1=EL1-ZET*TF1
ELL2=EL2-ZET*TF2
EM2=U*U+V*V
EM=SQRT(EM2)
ELLP=ELL1+ELL2
S=(ELL1-ELL2)/ELLP
AB=2.0*EM/ELLP
TAU=-DDD*SX/EN2
CPSI=SX*SQRTF(ELL1**2-DEL**2)/(ELL1*EN)
TAU1=TAU-ELL1*CPSI
TAU2=TAU+ELL2*CPSI
AQ=ATAN(U/V)
IF(V) 41,42,42
41 AQ=PI+AQ
GO TO 44
42 IF(U) 43,44,44
43 AQ=2.0*PI+AQ
44 AQ=AQ/DR
AC=ATAN(XI/ETA)
IF(ETA) 45,46,46
45 AC=PI+AC
GO TO 48
46 IF(XI) 47,48,48
47 AC=2.0*PI+AC
48 AC=AC/DR
AN=ATANF(DU/DV)
IF(DV) 31,32,32
31 AN=PI+AN
GO TO 34
32 IF(DU) 33,34,34
33 AN=2.0*PI+AN
34 AN=AN/DR
AV=AQ-AC
IF(AV) 49,51,51
49 AV=AV+360.0
51 AP=22.35-0.01*(TH+1.0)
AQP=AQ-AP
WEM=DDD/EN
WLD1=ELL1**2-DEL**2
WLD2=ELL2**2-DEL**2
IF(WLD2) 61,62,62
62 W2=WEM+SQRTF(WLD2)
T2=-W2*SX/EN
W1=WEM+SQRTF(WLD1)
T1=-W1*SX/EN
K=1
GO TO 65
61 IF(WLD1) 63,64,64
```

```
64 W1=WEM+SQRTF(WLD1)
T1=-W1*SX/EN
K=2
GO TO 65
63 K=3
65 IF(EM+ELL2) 11,11,12
11 AR=1.0
BB=0.0
EMM1=1.0
GO TO 30
12 IF(EM-ELL1) 13,13,14
14 AR=0.0
BB=360.0
EMM1=0.0
GO TO 30
13 CC=(ELL1**2+ELL2**2-2.0*EM2)/(ELL1**2-ELL2**2)
SC=SQRT(1.0-CC**2)
C=ATAN(SC/CC)
CB=(ELL1*ELL2+EM2)/(EM*ELLP)
SB=SQRT(1.0-CB**2)
B=ATAN(SQRT(1.0-CB**2)/CB)
IF(CC) 21,22,22
21 C=PI+C
22 IF(CB) 23,24,24
23 B=PI+B
24 BB=360.0-2.0*B/DR
EMM1=(ELL1-EM)/ELLP
A=PI-B-C
AR=(S*S*A+B-S*SC)/PI
30 PUNCH 97,TH,TM,TS
PUNCH 97,FLAT,FLONG,ALT
PUNCH 97,TAU,S,AB
PUNCH 97,EMM1,BB,AR
PUNCH 97,AQ,AV,AN
PUNCH 97,AC,AP,AOP
PUNCH 97,ELL1,ELL2,EM
PUNCH 97,EN,TAU1,TAU2
GO TO (66,67,68),K
66 PUNCH 97,DEL,WEM,W1
PUNCH 97,T1,W2,T2
GO TO 50
67 PUNCH 97,DEL,WEM,W1
PUNCH 97,T1
GO TO 50
68 PUNCH 97,DEL,WEM
50 PUNCH 90
GO TO 1
90 FORMAT(1H )
91 FORMAT(I2)
93 FORMAT(2F6.1,F8.3,F10.2,2F10.5)
94 FORMAT(I2,F8.0)
97 FORMAT(20X,3F11.6)
99 FORMAT(49H                                                  )
END
END PROG
```

Glossary

PI	π
SX	seconds per minute; minutes per hour
DR	radians per degree
F2	$[(\text{polar radius})/(\text{equatorial radius})]^2$, Hayford's spheroid
UO	μ, in radians
DO	d, in radians, from $\tan^{-1}[(\sin d)/(\cos d)]$
TF1	$\tan f_1$
TF2	$\tan f_2$
DUM	μ', in radians per hour
DD	d', in radians per hour
M	number of trajectory points to be calculated
TH	hour, universal time
TMO	minutes, ephemeris time, of Besselian elements
XO	x, at 1830 ET
X1	x, at 1840 ET
YO	y, at 1830 ET
Y1	y, at 1840 ET
EL10	ℓ_1 (penumbra), at 1830 ET
DEL1	(ℓ_1, at 1840 ET) - (ℓ_1, at 1830 ET)
EL20	ℓ_2 (umbra), at 1830 ET
DEL2	(ℓ_2, at 1840 ET) - (ℓ_2, at 1830 ET)
TM	minutes, UT
TS	seconds, UT

ALT	altitude, in km
FLONG	longitude, in degrees, positive toward west
FLAT	latitude, in degrees, positive toward north
TAU	minutes to maximum phase
S	radius of moon (solar radii)
AB	distance between center of sun and center of moon (solar radii)
EMM1	fraction of solar diameter covered by moon
BB	degrees on the solar rim not obscured by the moon
AR	fraction of solar disk obscured
AQ	angle (degrees) to the center of the moon east of the sun's north point
AV	angle (degrees) to the center of the moon east of the sun's vertex
AN	azimuth (degrees) of the eclipse axis path east of the sun's north point
AC	the parallactic angle (degrees), the angle to the vertex east of the north point
AP	angle (degrees) of the sun's north pole east of the sun's north point
AQP	angle (degrees) to the center of the moon east of the sun's north pole
ELL1	radius of penumbra (earth radii)
ELL2	radius of umbra (earth radii)
EM	distance (earth radii) from the observer to the eclipse axis
EN	hourly rate of change of EM
TAU1	minutes to first contact along eclipse axis path
TAU2	minutes to second contact along eclipse axis path

DEL	distance (earth radii) from the observer to the eclipse axis path
WEM	distance (earth radii) from the observer parallel to the eclipse axis path to the point of maximum phase
W1	distance (earth radii) from the observer parallel to the eclipse axis path to the penumbra (first contact)
T1	W1 in minutes
W2	distance (earth radii) from the observer parallel to the eclipse axis path to the umbra (second contact)
T2	W2 in minutes

The relation between these output values is shown schematically in Figures 1 and 2.

TABLE 1

BESSELIAN ELEMENTS OF THE TOTAL ECLIPSE OF THE SUN MARCH 7

E.T.		Intersection of Axis of Shadow with Fundamental Plane		Direction of Axis of Shadow			Radius of Shadow on Fundamental Plane	
		x	y	sin d	cos d	μ	Penumbra	Umbra
h	m					°		
15	00	−1.548751	−0.333523	−0.092008	0.995758	42.21379	0.539158	−0.007152
	10	1.464521	0.287708	.091963	.995762	44.71441	.539180	.007130
	20	1.380288	0.241891	.091918	.995767	47.21503	.539202	.007109
	30	1.296054	0.196072	.091873	.995771	49.71566	.539223	.007088
	40	1.211817	0.150251	.091828	.995775	52.21628	.539243	.007068
	50	1.127577	0.104429	.091783	.995779	54.71690	.539263	.007048
16	00	−1.043337	−0.058605	−0.091738	0.995783	57.21753	0.539282	−0.007029
	10	0.959095	−0.012780	.091693	.995787	59.71815	.539300	.007011
	20	0.874852	+0.033046	.091648	.995791	62.21877	.539317	.006994
	30	0.790607	0.078873	.091603	.995796	64.71940	.539334	.006977
	40	0.706363	0.124701	.091558	.995800	67.22002	.539350	.006961
	50	0.622117	0.170529	.091513	.995804	69.72064	.539365	.006946
17	00	−0.537871	+0.216359	−0.091468	0.995808	72.22126	0.539380	−0.006932
	10	0.453625	0.262190	.091423	.995812	74.72189	.539394	.006918
	20	0.369379	0.308021	.091378	.995816	77.22251	.539407	.006905
	30	0.285134	0.353853	.091333	.995820	79.72314	.539419	.006892
	40	0.200889	0.399686	.091288	.995825	82.22376	.539431	.006880
	50	0.116645	0.445519	.091243	.995829	84.72438	.539442	.006869
18	00	−0.032402	+0.491352	−0.091198	0.995833	87.22501	0.539453	−0.006859
	10	+0.051840	0.537185	.091153	.995837	89.72563	.539462	.006850
	20	0.136080	0.583018	.091108	.995841	92.22626	.539471	.006841
	30	0.220318	0.628851	.091063	.995845	94.72688	.539479	.006832
	40	0.304554	0.674683	.091018	.995849	97.22750	.539487	.006825
	50	0.388787	0.720515	.090973	.995853	99.72813	.539494	.006818
19	00	+0.473019	+0.766347	−0.090928	0.995857	102.22875	0.539500	−0.006812
	10	0.557248	0.812177	.090883	.995862	104.72937	.539505	.006807
	20	0.641474	0.858007	.090838	.995866	107.23000	.539510	.006802
	30	0.725697	0.903835	.090793	.995870	109.73062	.539514	.006798
	40	0.809917	0.949662	.090748	.995874	112.23125	.539518	.006795
	50	0.894134	0.995488	.090703	.995878	114.73187	.539520	.006792
20	00	+0.978347	+1.041312	−0.090658	0.995882	117.23250	0.539522	−0.006790
	10	1.062555	1.087134	.090613	.995886	119.73312	.539523	.006789
	20	+1.146760	+1.132955	−0.090568	0.995890	122.23375	0.539524	−0.006788

tan f_1 0.004710
tan f_2 0.004687
μ' 0.261865 radians per hour
d' +0.000271 radians per hour

Sample Input

```
LIS FL147
005* 14.147 TRAJECTORY
010 15
020 38. 54.5 50. 75.2317 37.6188
030 39. 3.5 60. 75.1672 37.5608
040 39. 13.5 70. 75.1006 37.5007
050 39. 25. 80. 75.028 37.4347
060 39. 38. 90. 74.9426 37.3567
070 39. 53. 100. 74.8449 37.2669
080 40. 13. 110. 74.716 37.1471
090 40. 55. 119. 74.449 36.8958
100 41. 40. 110. 74.1661 36.6229
110 42. 0. 100. 74.0404 36.5011
120 42. 10. 90. 73.9768 36.4402
130 42. 17.5 80. 73.9271 36.3908
140 42. 29. 70. 73.8572 36.3232
150 42. 49. 60. 73.7321 36.1992
160 42. 58. 50. 73.6744 36.1439
```

Sample Output

18.000000	38.000000	54.500000
37.618800	75.231700	50.000000
-.115953	1.038120	.024840
1.000000	0	1.000000
130.641166	107.033708	47.774209
23.607458	22.160000	108.481166
.536266	-.010030	.006536
.419949	-76.729087	-1.548891
.006485	.000812	.537038
-76.729087	.008463	-1.209153

Output Format

TH	TM	TS
FLAT	FLONG	ALT
TAU	S	AB
EMM1	BB	AR
AQ	AV	AN
AC	AP	AQP
ELL1	ELL2	EM
EN	TAU1	TAU2
DEL	WEM	W1
T1	W2	T2

01CB316-10E

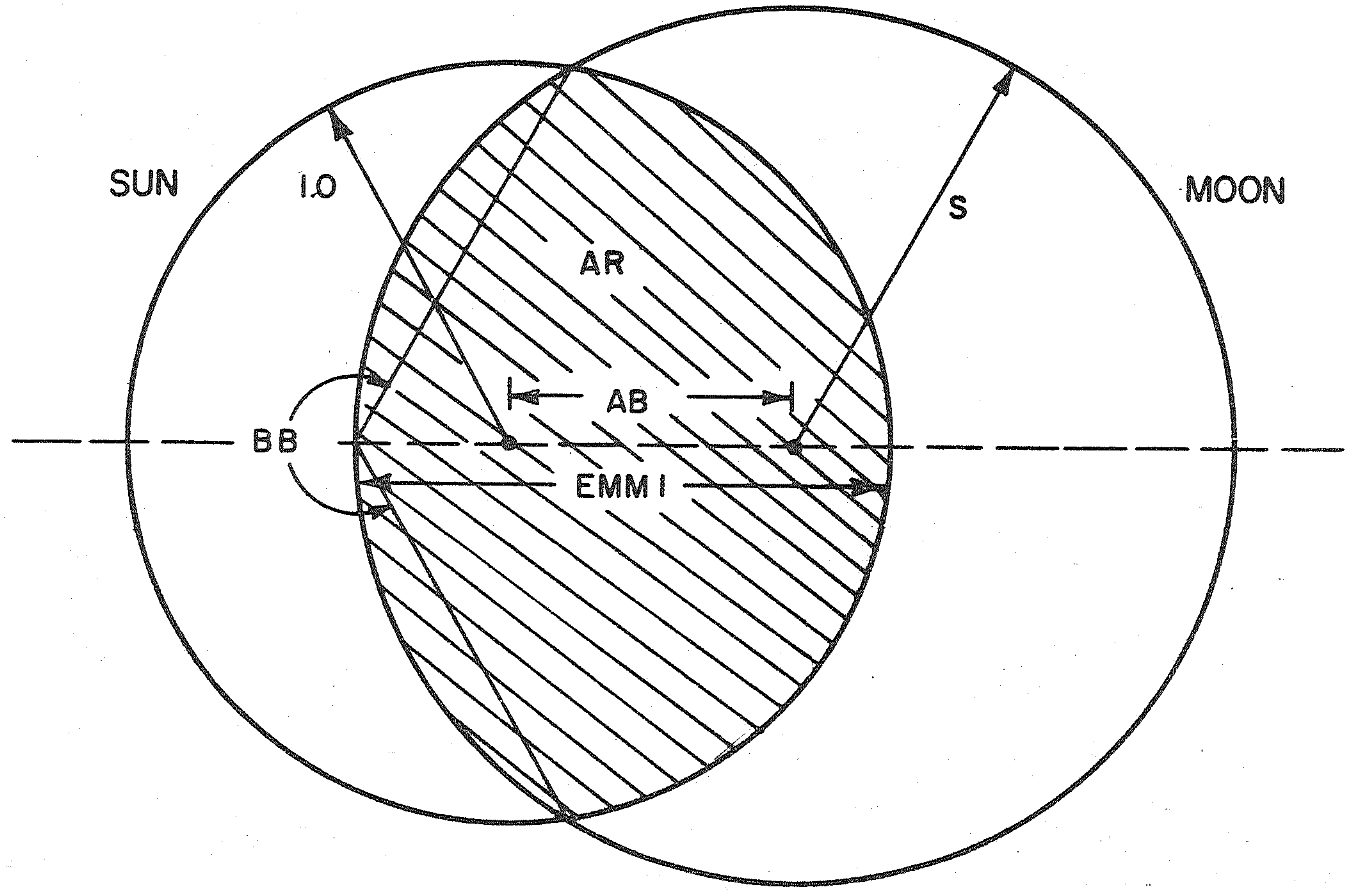

FIGURE 1

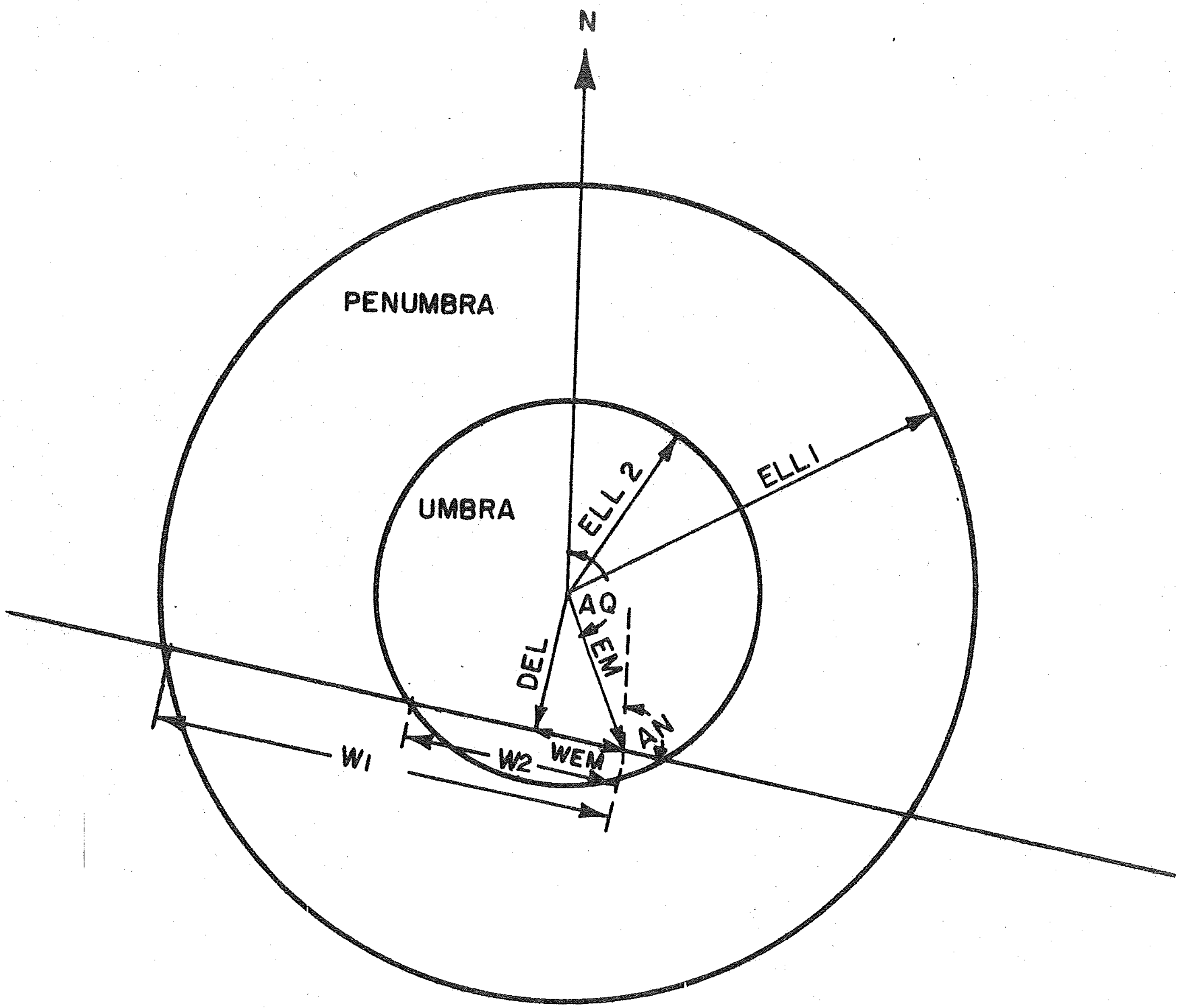

FIGURE 2